https://doi.org/10.15407/ujpe66.3.198

O.O. PRIKHODKO,[1] Y.M. BIDASYUK [2]

[1] Taras Shevchenko National University of Kyiv, Department of Physics
(64/13, Volodymyrs'ka Str., Kyiv 01601, Ukraine; e-mail: eap@univ.kiev.ua)
[2] Physikalisch-Technische Bundesanstalt
(Bundesallee 100, D-38116 Braunschweig, Germany; e-mail: yuriy.bidasyuk@ptb.de)

PROJECTED GROSS–PITAEVSKII EQUATION FOR RING-SHAPED BOSE–EINSTEIN CONDENSATES

We propose an alternative implementation of the projected Gross–Pitaevskki equation adapted for a numerical modeling of the atomic Bose–Einstein condensate trapped in a toroidally shaped potential. We present an accurate efficient scheme to evaluate the required matrix elements and to calculate the time evolution of the matter wave field. We analyze the stability and accuracy of the developed method for equilibrium and nonequilibrium solutions in a ring-shaped trap with an additional barrier potential corresponding to recent experimental realizations.

K e y w o r d s: Bose–Einstein condensation, Gross–Pitaevskii equation, spectral methods.

1. Introduction

The Gross–Pitaevskii equation (GPE) is the most widely used mathematical tool to model atomic Bose–Einstein condensates (BEC) and their dynamics at zero temperature [1, 2]. Various modifications have been proposed to extend the applicability of GPE for a nonperturbative treatment of finite temperature effects and nonequillibrium dynamics. Such methods are commonly termed classical-field (or C-field) methods. Most notable methods of this class are truncated Wigner approximation [3] and the projected Gross–Pitaevskii equation (PGPE) [4, 5]. The latter will be the main focus of the present work. A wide range of physical problems addressed with PGPE and its modifications includes, in particular, the Bose-condensation and quasicondensation [6–8], dynamical generation [9] and decay [10] of quantum vortices, and dissipative bosonic Josephson effect [11].

From the numerical point of view, the projected Gross–Pitaevskii equation belongs to the class of pseudospectral methods. It relies on the reformulation of the GPE in the spectral basis of single-particle states, and the frequent transformations between coordinate and spectral representations are at the core of the numerical procedure. Such an approach requires explicit knowledge of the basis states in order to efficiently transform the condensate wave function between the two representations. It is therefore quite natural that existing realizations of PGPE are based on the eigenstates of a three-dimensional harmonic oscillator potential [4, 5, 12]. This limits the applicability of such realizations to the traps which can be well approximated by the harmonic oscillator and account for any nonharmonic part as a small perturbation.

In the present work, we propose an extension of the PGPE formalism to describe the Bose–Einstein condensates trapped in toroidally shaped traps. While the single particle states of a toroidal trap cannot be obtained analytically, we show here that PGPE can be formulated equally well in terms of approximate eigenstates and produce physically relevant results. We verify the accuracy and time stability of the developed approach and demonstrate that the made approximations do not introduce significant errors. The developed approach can be straightforwardly extended to include dynamical noise terms and to solve the stochastic projected Gross–Pitaevskii equation (SPGPE). This will allow us to model a dynamical evolution of finite-temperature toroidal condensates.

2. PGPE Model for a Toroidal System

We consider a system that is characterized by the mean-field Gross–Pitaevskii Hamiltonian operator $H_{\rm GP}$ [1, 2]:

$$H_{\rm GP}\,\psi(\mathbf{r},t) = \Big[-\frac{\hbar^2\nabla^2}{2M} + V_{\rm trap}(\mathbf{r}) + \delta V(\mathbf{r},t) + g|\psi(\mathbf{r},t)|^2 \Big]\psi(\mathbf{r},t). \quad (1)$$

with the nonlinear interaction parameter $g = 4\pi\hbar^2 a/M$, where a is the s-wave scattering length, and M is the atom mass. The potential $V_{\rm trap}(\mathbf{r})$ is a cylindrically symmetric ring-shaped trap formed by a combination of a shifted harmonic potential in the radial direction and another harmonic potential in the vertical direction [13, 14]:

$$V_{\rm trap}(\mathbf{r}) = \frac{M}{2}\left[\omega_r^2(r-r_0)^2 + \omega_z^2 z^2\right], \tag{2}$$

where we use cylindrical coordinates $\mathbf{r} = \{r, \theta, z\}$, $r = \sqrt{x^2+y^2}$. The additional time-dependent potential $\delta V(\mathbf{r}, t)$ is considered as a (small) perturbation to the trap potential. It can represent, for example, a moving barrier as in experiments of Refs. [14, 15].

The classical field or C-field methods are based on the concept of splitting the many-particle system into highly occupied low-energy modes described by the coherent classical field $\psi(\mathbf{r}, t)$ and sparsely occupied incoherent high-energy modes forming a thermal bath. Such splitting is conveniently represented in the basis of single-particle eigenstates ϕ_n of the trapping potential $V_{\rm trap}$

$$H_0\phi_\alpha = \left[-\frac{\hbar^2\nabla^2}{2M} + V_{\rm trap}(\mathbf{r})\right]\phi_\alpha = E_\alpha\phi_\alpha, \tag{3}$$

where α represents a set of quantum numbers that characterize the single-particle eigenstates ϕ_α. The classical field $\psi(\mathbf{r}, t)$ is then a coherent superposition of these states with energies below the chosen cut-off energy $e_{\rm cut}$

$$\psi(\mathbf{r}, t) = \sum_{\alpha\in C} c_\alpha(t)\phi_\alpha(\mathbf{r}), \tag{4}$$
$$C = \{\alpha \colon E_\alpha \le e_{\rm cut}\}.$$

The choice of the cut-off energy may be a complicated problem for finite temperature calculations (see, e.g., [16, 17]). In the case of zero temperature, this parameter only determines the basis size and the overall accuracy of decomposition (4).

Unfortunately, for the ring-shaped potential (2), we cannot solve the single-particle problem (3) analytically. Instead we can choose a basis that only approximately diagonalizes the Hamiltonian H_0. We define the basis states for the ring-shaped system as

$$\phi_\alpha(r, \theta, z) = \frac{1}{\sqrt{2\pi r}}\varphi_n^{(\omega_r)}(r-r_0)\varphi_m^{(\omega_z)}(z)e^{il\theta}, \tag{5}$$

where α contains now three quantum numbers $\alpha \to \{n, l, m\}$, and $\varphi_n^{(\omega)}(x)$ are normalized eigenstates of a one-dimensional harmonic oscillator with frequency ω:

$$\varphi_n^{(\omega)}(x) = \sqrt{\frac{b}{2^n\sqrt{\pi}n!}}H_n\left(\frac{x}{b}\right)e^{-\frac{x^2}{2b^2}},$$

where $b = \sqrt{\hbar/M\omega}$ is the characteristic oscillator length, H_n is the Hermite polynomial of the order n. This basis (5) is not orthonormalized due to its radial dependence. The approximate orthogonality can be ensured, if $\sqrt{\hbar/M\omega_r} \ll r_0$ (see Appendix A for more details). The Hamiltonian H_0 is also not fully diagonalized by the chosen basis, but rather takes the form

$$\langle\phi_{n'l'm'}|H_0|\phi_{nlm}\rangle =$$
$$= \left[(E_n^{(r)} + E_m^{(z)})\delta_{nn'} + E_l^{(\theta)}I_{nn'}\right]\delta_{mm'}\delta_{ll'},$$

where

$$E_n^{(r)} = \hbar\omega_r\left(n+\frac{1}{2}\right), \quad E_m^{(z)} = \hbar\omega_z\left(m+\frac{1}{2}\right),$$
$$E_l^{(\theta)} = \frac{\hbar^2}{2Mr_0^2}\left(l^2-\frac{1}{4}\right),$$
$$I_{nn'} = \int_0^\infty dr\frac{r_0^2}{r^2}\varphi_n^{(\omega_r)}(r-r_0)\varphi_{n'}^{(\omega_r)}(r-r_0). \tag{6}$$

The matrix element $I_{nn'}$ formally diverges at $r \to 0$. It can still be meaningfully approximated, if we restrict the integration to the region of finite support of the oscillator functions and use again the condition $\sqrt{\hbar/M\omega_r} \ll r_0$ (see Appendix B for more details). In this case, $I_{nn'}$ is also close to the identity matrix, and we can approximately define the single-particle energy spectrum as

$$E_{nml} = E_n^{(r)} + E_m^{(z)} + E_l^{(\theta)}. \tag{7}$$

Using this approximate spectrum and the chosen cut-off energy, we define the C-region and truncate basis (4)

$$C = \{n, m, l : E_n^{(r)} + E_m^{(z)} + E_l^{(\theta)} \le e_{\rm cut}\},$$

which also fixes the maximal value of each of the quantum numbers $n_{\max}$, $m_{\max}$, $l_{\max}$.

The density of states which corresponds to spectrum (7) can be calculated analytically as follows:

$$\rho(\epsilon) = \frac{4}{3}\frac{\sqrt{2M}r_0}{\hbar^3\omega_r\omega_z}\,\epsilon^{3/2}. \tag{8}$$

More details on this derivation can be found in Appendix C.

The density of states can be also estimated in the quasiclassical approximation

$$\rho_{qc}(\epsilon) = \int \frac{d\mathbf{r}d\mathbf{p}}{(2\pi\hbar)^3}\delta(\epsilon - E(\mathbf{r},\mathbf{p})) = \\ = \frac{M^{3/2}}{\sqrt{2}\pi^2\hbar^3}\int\limits_{V\le\epsilon} d\mathbf{r}\sqrt{\epsilon - V(\mathbf{r})}, \tag{9}$$

where $E(\mathbf{r},\mathbf{p})$ is the energy of a classical particle in the potential $V(\mathbf{r}) = V_{\rm trap}(\mathbf{r}) + \delta V(\mathbf{r})$. The integral in (9) can be calculated analytically for the pure ring trap potential (2) and energies $\epsilon < M\omega_r^2 r_0^2/2$ producing the same expression as above. In general, the closeness of estimates (8) and (9) shows how good the real spectrum of Eq. (3) is reproduced by the approximate basis states (5). From the density of states (8), one may also see that the number of basis states in C-region (and, consequently, the numerical complexity of the calculations) grows with the cut-off as $N_C \sim e_{\rm cut}^{5/2}$.

If we completely neglect the incoherent region (all single-particle states above the cut-off), then the classical field $\psi(\mathbf{r},t)$ will be a solution to the projected Gross–Pitaevskii equation (PGPE) [5, 12]:

$$i\hbar\frac{\partial\psi(\mathbf{r},t)}{\partial t} = \mathcal{P}H_{\rm GP}\psi(\mathbf{r},t), \tag{10}$$

where $\mathcal{P}$ is a projection operator to the C-space

$$\mathcal{P}\psi(\mathbf{r},t) = \sum_{\alpha\in C}\phi_\alpha(\mathbf{r})\int d\mathbf{r}'\phi_\alpha^*(\mathbf{r}')\psi(\mathbf{r}',t).$$

In the spectral basis, the equation for expansion coefficients c_α reads

$$i\hbar\frac{dc_\alpha}{dt} = (E_n^{(r)} + E_m^{(z)})c_\alpha + E_l^{(\theta)}D_\alpha + F_\alpha, \tag{11}$$

where

$$D_\alpha = \int d\mathbf{r}\phi_\alpha^*(\mathbf{r})\frac{r_0^2}{r^2}\psi(\mathbf{r},t), \tag{12}$$

$$F_\alpha = \int d\mathbf{r}\phi_\alpha^*(\mathbf{r})\left[\delta V(\mathbf{r},t) + g|\psi(\mathbf{r},t)|^2\right]\psi(\mathbf{r},t). \tag{13}$$

In order to numerically solve Eq. (11), we need an efficient accurate way to transform the solution between the coordinate and spectral representations. The integrals containing harmonic oscillator states can be accurately approximated by the Gauss–Hermite quadrature. The general form of the N_Q point quadrature rule is

$$\int\limits_{-\infty}^{\infty} dx e^{-x^2} f(x) \approx \sum_{j=1}^{N_Q} w_j f(x_j),$$

where x_j and w_j are the quadrature points and weights. This quadrature rule is exact, if $f(x)$ is a polynomial with degree below $2N_Q - 1$. The transformation of any function $\psi(\mathbf{r})$ to the basis representation is then constructed as follows:

$$c_{nlm} = \int d\mathbf{r}\phi_{nlm}^*(\mathbf{r})\psi(\mathbf{r}) = \\ = \sum_{jks} w_j^{(r)}w_s^{(z)}\delta\theta U_{jn}\,W_{kl}^*\,Y_{sm}\psi(r_j,\theta_k,z_s),$$

where we introduce the rescaled quadrature weights

$$w_j^{(r)} = w_j b_r e^{(r_j - r_0)^2/b_r^2}, \quad w_s^{(z)} = w_s b_z e^{r_s^2/b_z^2},$$

with

$$b_r = \sqrt{\frac{\hbar}{M\omega_r}}, \quad b_z = \sqrt{\frac{\hbar}{M\omega_z}}.$$

The integration in the azimuthal direction is performed with a usual trapezoidal rule on a uniform grid with spacing $\delta\theta$. The transformation matrices are defined as the basis states evaluated on the quadrature grid:

$$U_{jn} = \varphi_n^{(\omega_r)}(r_j - r_0), \quad W_{kl} = e^{il\theta_k}, \quad Y_{sm} = \varphi_m^{(\omega_z)}(z_s).$$

The backward transformation to the spatial representation is then performed as follows:

$$\psi(r_j,\theta_k,z_s) = \sum_{nml} U_{jn}\,W_{kl}\,Y_{sm}\,c_{nlm}.$$

For more details on the transformations between the coordinate and spectral representations and the calculation of matrix elements, we refer to Ref. [12]. It is worth noting that, in practical realizations, the

transformation with the matrix W_{kl} can be replaced with a Fast Fourier Transform for a better performance. We however prefer to keep this transformation matrix here for clarity.

In order to perform a time evolution of Eq. (11), we build a computational scheme similar to the split-step Fourier transform (SSFT) method which is widely used for the GPE modeling [18]. This method implements a time evolution operator $\exp(-iH_{\rm GP}t/\hbar)$ to propagate the condensate wave function in time. Adapting this scheme to PGPE (11) and using a second-order Trotter decomposition for the time evolution operator, a basic time evolution step $c_{nlm}(t) \to$ $\to c_{nlm}(t+\delta t)$ can be outlined as the following sequence:

$$1\colon\ c'_{nlm} = \exp\left[-\frac{i\delta t}{2\hbar}(E_n^{(r)} + E_m^{(z)})\right] c_{nlm}(t),$$

$$2\colon\ d_{jlm} = \exp\left[-\frac{i\delta t}{2\hbar}E_l^{(\theta)}\frac{r_0^2}{r_j^2}\right] \sum_n U_{jn} c'_{nlm},$$

$$3\colon\ f_{jks} = \sum_{lm} W_{kl} Y_{sm} d_{jlm},$$

$$4\colon\ f'_{jks} = \exp\left[-\frac{i\delta t}{\hbar}\left(\delta V(r_j,\theta_k,z_s,t) + g|f_{jks}|^2\right)\right] f_{jks},$$

$$5\colon\ d'_{jlm} = \sum_{ks} w_s^{(z)} \delta\theta\, W^*_{kl} Y_{sm} f'_{jks},$$

$$6\colon\ c''_{nlm} = \sum_j w_j^{(r)} U_{jn} \exp\left[-\frac{i\delta t}{2\hbar}E_l^{(\theta)}\frac{r_0^2}{r_j^2}\right] d'_{jlm},$$

$$7\colon\ c_{nlm}(t+\delta t) = \exp\left[-\frac{i\delta t}{2\hbar}(E_n^{(r)} + E_m^{(z)})\right] c''_{nlm}.$$

We note that, in order to calculate the term which includes the integral D_α defined by Eq. (12), we need to perform a partial transformation and use the coordinate representation in r together with a spectral representation in θ and z.

3. Numerical Verification

In order to test the developed numerical approach, we model the toroidal trap of the experiment [14]. The parameters of the trap potential are then defined as follows: $\omega_r/2\pi = 188$ Hz, $\omega_z/2\pi = 472$ Hz, $r_0 = 19.5\,\mu$m. The total number of atoms in BEC is $N = 4\times10^5$, and the corresponding chemical potential is estimated as $\mu \approx 10\hbar\omega_r$. The barrier is approximated

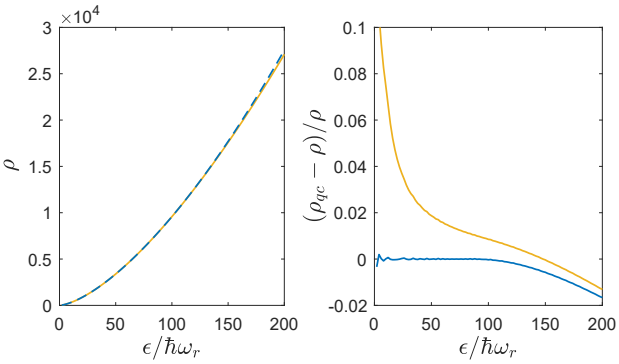

Fig. 1. Left panel: Density of states for the ring-shaped potential without a barrier from Eq. (8) (dashed blue line) and (9) (solid yellow line). Right panel: Blue (dark grey) line shows relative error of Eq. (8) for a homogeneous ring, yellow (light grey) line is the same, but for a ring with additional barrier potential

by the following potential which is considered as time-independent for the purposes of the present study:

$$\delta V(\mathbf{r}) = V_b \Theta(x) e^{-\frac{y^2}{2\lambda^2}},$$

where $\Theta(x)$ is the Heaviside step function, $\lambda = 6\mu$m is the $1/e^2$ half-width of the barrier, and we choose the barrier height to match the value of the chemical potential $V_b = 10\hbar\omega$.

The main requirement for the validity of our approach is $b_r \ll r_0$. For the trap parameters defined above, we get $b_r/r_0 \approx 0.04$. First, we test the quality of our basis representation by evaluating the density of states and comparing it to the analytic expression (8). The result is shown in Fig. 1. It shows that the energy spectrum of a toroidal trap (without a barrier) is reproduced very accurately for energies up to $100\hbar\omega_r$. The discrepancy is expectedly higher, when the barrier potential is taken into account. The relative error is, however, within 2% in the high-energy region, which is very good for such a simple approximation and justifies the cut-off definition based on the the approximate spectrum (7).

Next, we calculate the ground state of the system with a barrier by propagating PGPE (11) in the imaginary time. This is done for different values of e_{cut} to see the effect of a basis size on the accuracy of the calculated ground state. The results are shown in Fig. 2. In order to estimate the error, we compare the coordinate space representation of the obtained solutions to the solution of a three-dimensional GPE obtained on a very dense coordinate grid with the

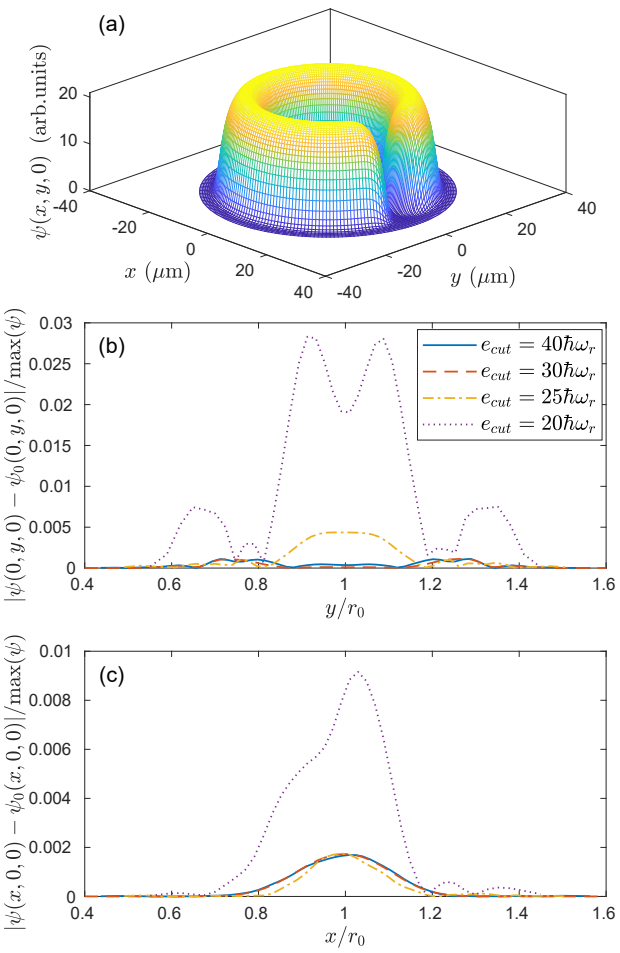

Fig. 2. Ground state solution of PGPE on the quadrature points in the $z = 0$ plane (a). Relative error of the solution in ccoordinate space along the radial direction away from the barrier for four different values of the energy cut-off and, consequently, different basis sizes: $e_{\rm cut} = 20\hbar\omega_r$ (7282 basis states), $e_{\rm cut} = 25\hbar\omega_r$ (12576 basis states), $e_{\rm cut} = 30\hbar\omega_r$ (19676 basis states), $e_{\rm cut} = 40\hbar\omega_r$ (39970 basis states) (b). Same as (b) but along the barrier direction (c)

usual SSFT method. We see that, for all chosen values of the cut-off energy, our numerical procedure produces reasonable approximations of the condensate ground state. The error converges rapidly with increasing the basis size and reaches saturation around $e_{\rm cut} = 30\hbar\omega_r$. We conclude that this is the optimal cut-off energy for such system and use only this value for the rest of this section. It is worth noting that, in realistic finite-temperature calculations, the choice of the cut-off energy is a nontrivial problem, and its definition is related to the temperature of the system [10, 11, 19]. For the purposes of the present feasibility study, which does not address any real finite-temperature processes, the cut-off value is considered only as a measure of the basis size and, consequently, the quality of a spectral representation of the condensate wave function.

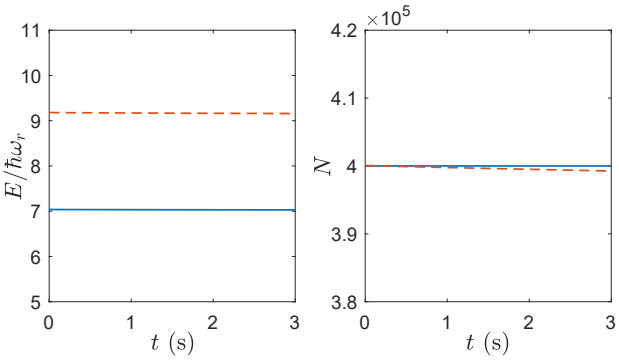

Fig. 3. Energy per particle (Left panel) and the total number of atoms (Right panel) monitored during the real time evolution of PGPE. The initial state for the evolution is chosen as equilibrium state (solid blue lines) or a nonequilibrium state (dashed red lines) with the same initial number of particles

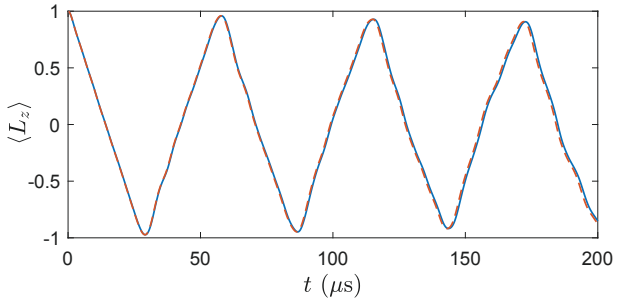

Fig. 4. Evolution of the angular momentum projection $\langle L_z \rangle$ modeled with PGPE (solid blue line) and grid-based GPE (dashed red line)

While PGPE, in general, conserves the total energy and the normaization of the wave function (which is the total number of particles in the system), we cannot prove that this conservation laws are preserved in basis (5) which is only approximately orthogonal. This may lead to an accumulation of numerical errors and, as a result, to a drift of the conserved quantities. Such effects can be even stronger in the presence of the barrier potential, as the single particle spectrum is shifted. We therefore check next that the energy and the atom number are reasonably conserved on a time scale of the experiment which is around 3 seconds in [14]. In order to prepare a nonequilib-

rium state, we add a random complex noise uniformly distributed across all basis states to the stationary state. We then renormalize the obtained state to get a state with the same number of atoms, but with the higher energy than the ground state. Figure 3 shows the evolution of the energy per particle and the number of particles in time for the initial equilibrium and nonequilibrium states. The relative drift of these quantities on the time scale of the experiment is about 0.2% for the nonequilibrium state. In the evolution of the stationary state, no noticeable drift is observed. Stability of the conserved quantities even for nonequilibrium states shows the applicability of the proposed time evolution scheme and the overall consistency of the developed algorithm on physically relevant time scales.

We perform the next test in order to further verify the accuracy of the nonequilibrium dynamics reproduced by our evolution scheme. We prepare the initial state by adding a phase circulation to the stationary ground state introducing a single quantum of the angular momentum to the system. The time evolution of such state efficiently mimics the instability of persistent current states in a ring with a barrier. As our equation does not contain any explicit dissipation mechanism, such instability manifests as oscillations of the average angular momentum projection $\langle L_z \rangle$. Such unstable evolution was modeled with our evolution scheme of PGPE and with the grid-based GPE for comparison (see Fig. 4). We see a nearly perfect match of the two results. It is worth mentioning that the value of $\langle L_z \rangle$ can be calculated in the basis representation exactly, as the basis states (5) are eigenfunctions of the L_z operator.

4. Conclusions

We have developed an implementation of the projected Gross–Pitaevskii equation adapted for Bose–Einstein condensates in toroidal traps. It is based on approximate eigenstates of a single-particle Hamiltonian which nevertheless closely reproduces the spectrum of the trap.

We have also proposed a time propagation scheme for PGPE which is similar to the well-established split-step Fourier transform method. This scheme can be applied to both real and imaginary time evolutions of PGPE. It was thoroughly tested and is shown to produce stable and accurate results. Such fully explicit time evolution algorithm is straightforward to complement with time-dependent noise terms and to realize the stochastic projected Gross–Pitaevskii equation. This will allow the modeling of various fintie-temperature processes in BEC which is the main application of PGPE models. We therefore believe that the proposed method can be especially useful for the modeling of the temperature-induced decay of persistent currents in BEC and will help to resolve the existing discrepancies between theory and experiment [14, 15, 20, 21].

From the performance point of view, the advantage of PGPE is that it needs to be propagated on a relatively small prescribed basis, much smaller than the typical number of points in three-dimensional grid-based calculations. For the chosen value of the cut-off energy, the basis size is about 20 k states. If compared to grid-based calculations, the minimally acceptable three-dimensional grid size for the system under study can be estimated as $128 \times 128 \times 32$, which leads to more that 500 k grid points. On the other hand, however, the effect of a small basis size for PGPE is compensated by the additional computational cost of frequent transformations. Without performing a detailed performance study, we only note that the practical computational times were comparable for our implementations of PGPE and grid-based GPE.

APPENDIX A
Approximate Orthogonality of the Basis

Basis (5) is only approximately orthonormalized due to its radial dependence. The overlap integral of two basis functions is

$$S_{\alpha\alpha'} = \iiint r dr\, d\theta\, dz \phi_\alpha(r,\theta,z)\phi_{\alpha'}(r,\theta,z) =$$

$$= \delta_{ll'}\delta_{mm'} \int_0^\infty dr \varphi_n^{(\omega_r)}(r-r_0)\varphi_{n'}^{(\omega_r)}(r-r_0) =$$

$$= \delta_{ll'}\delta_{mm'} \int_{-r_0}^\infty dr \varphi_n^{(\omega_r)}(r)\varphi_{n'}^{(\omega_r)}(r). \tag{A1}$$

The oscillator functions have finite support defined by the classical turning points $R_n = \sqrt{\frac{2n\hbar}{M\omega_r}}$. Outside these points, the function is exponentially small. Therefore, if $r_0 > R_n, R_{n'}$, then we can approximate the overlap integral as follows

$$S_{\alpha\alpha'} = \delta_{ll'}\delta_{mm'} \left[\delta_{nn'} - \int_{-\infty}^{-r_0} dr \varphi_n^{(\omega_r)}(r)\varphi_{n'}^{(\omega_r)}(r) \right] =$$

$$= \delta_{ll'}\delta_{mm'} \left[\delta_{nn'} + \mathcal{O}\left(\left(\frac{r_0}{b_r}\right)^{n+n'} e^{-(\frac{r_0}{b_r})^2} \right) \right] \approx \delta_{\alpha\alpha'}, \tag{A2}$$

where $b_r = \sqrt{\hbar/M\omega_r} \ll r_0$ is a necessary requirement for approximate orthogonality.

APPENDIX B
Matrix $I_{nn'}$ and the Approximate Spectrum

Here, we analyze the matrix elements $I_{nn'}$ defined by (6) and show the validity of the approximate spectrum (7). More specifically, in order to define the cut-off energy, we need to approximate the high-energy region of the spectrum. Therefore, we are interested mainly in the behavior of $I_{nn'}$ for $n, n' \gg 1$. In this region, the basis functions are rapidly oscillating, and integral (6) can be approximated using stationary phase arguments [22, 23]:

$$I_{nn'} = \int_0^\infty dr \frac{r_0^2}{r^2} \varphi_n^{(\omega_r)}(r - r_0)\varphi_{n'}^{(\omega_r)}(r - r_0) \approx$$

$$\approx \delta_{nn'} \frac{1}{2} \left[\frac{r_0^2}{(r_0 + R_n)^2} + \frac{r_0^2}{(r_0 - R_n)^2} \right] \approx$$

$$\approx \delta_{nn'} \left[1 + 3\frac{R_n^2}{r_0^2} \right], \tag{B1}$$

where $R_n = \sqrt{\frac{2n\hbar}{M\omega_r}}$ are the classical turning points of the oscillator states, which are, at the same time, the points of stationary phase. The approximation is only valid, if the integrand r_0^2/r^2 is a smooth continuous function, and both points of stationary phase are within the integration region. This imposes the additional restriction $R_n < r_0$. With result (B1), we get the following spectrum:

$$E_{nml} = E_n^{(r)} + E_m^{(z)} + E_l^{(\theta)} + 3\hbar\omega_r \frac{b_r^4}{r_0^4} n \left(l^2 - \frac{1}{4} \right),$$

where $b_r = \sqrt{\hbar/M\omega_r}$. The condition $b_r \ll r_0$, which was imposed to ensure the orthogonality of the basis states, allows us to neglect the last term and to justify the approximate spectrum (7).

APPENDIX C
Derivation of the Density of States

Here, we show the relations between the density of states (8), the approximate spectrum (7), and the quasiclassical integral (9). We start with the spectrum (7):

$$E_{nml} = \hbar\omega_r \left(n + \frac{1}{2} \right) + \hbar\omega_z \left(m + \frac{1}{2} \right) +$$

$$+ \frac{\hbar^2}{2Mr_0^2} \left(l^2 - \frac{1}{4} \right).$$

We are mostly interested in the high-energy behavior of the spectrum. Therefore, to simplify the calculations we shift the spectrum so that the ground state ($n = m = l = 0$) has zero energy:

$$\tilde{E}_{nml} = \hbar\omega_r n + \hbar\omega_z m + \frac{\hbar^2 l^2}{2Mr_0^2}.$$

The number of states with energies $\tilde{E} < \epsilon$ is defined as the sum

$$N(\epsilon) = \sum_{\tilde{E}_{nml} < \epsilon} 1.$$

The simplest way to calculate this sum is to consider n, m, and l as continuous variables and convert it to the integral

$$N(\epsilon) = \iiint_{\tilde{E}_{nml} < \epsilon} dn\, dm\, dl.$$

This integral yields

$$N(\epsilon) = \frac{8}{15} \frac{\sqrt{2M} r_0}{\hbar^3 \omega_r \omega_z} \epsilon^{5/2}. \tag{C1}$$

The density of states is then calculated as the derivative of the above expression:

$$\rho(\epsilon) = \frac{dN(\epsilon)}{d\epsilon} = \frac{4}{3} \frac{\sqrt{2M} r_0}{\hbar^3 \omega_r \omega_z} \epsilon^{3/2}. \tag{C2}$$

Another approach to calculate the density of states is based on the quasiclassical approximation. The energy of the classical particle in the potential $V(\mathbf{r}) = V_{\text{trap}}(\mathbf{r})$ is

$$E(\mathbf{r}, \mathbf{p}) = \frac{p^2}{2M} + V(\mathbf{r}) = \frac{p^2}{2M} + \frac{M}{2} \left[\omega_r^2 (r - r_0)^2 + \omega_z^2 z^2 \right].$$

The density of states is then defined by the following integral:

$$\rho_{qc}(\epsilon) = \int \frac{d\mathbf{r} d\mathbf{p}}{(2\pi\hbar)^3} \delta(\epsilon - E(\mathbf{r}, \mathbf{p})) =$$

$$= \frac{M}{\pi^2\hbar^3} \int\limits_{V \le \epsilon} d\mathbf{r} \int dp\, p^2 \delta\left(p^2 - 2M[\epsilon - V(\mathbf{r})] \right) =$$

$$= \frac{M^{3/2}}{\sqrt{2}\pi^2\hbar^3} \int\limits_{V \le \epsilon} d\mathbf{r} \sqrt{\epsilon - V(\mathbf{r})} =$$

$$= \frac{M^{3/2}}{\sqrt{2}\pi^2\hbar^3} \int\limits_{V \le \epsilon} d\mathbf{r} \sqrt{\epsilon - M/2 \left[\omega_r^2 (r - r_0)^2 + \omega_z^2 z^2 \right]} =$$

$$= \frac{2\sqrt{2M} r_0 \epsilon^{3/2}}{\pi\hbar^3 \omega_r \omega_z} \int\limits_{\tilde{r}^2 + \tilde{z}^2 \le 1} d\tilde{r} d\tilde{z} \sqrt{1 - \tilde{r}^2 - \tilde{z}^2} =$$

$$= \frac{2\sqrt{2M} r_0 \epsilon^{3/2}}{\pi\hbar^3 \omega_r \omega_z} \frac{2}{3}\pi = \frac{4}{3} \frac{\sqrt{2M} r_0}{\hbar^3 \omega_r \omega_z} \epsilon^{3/2}, \tag{C3}$$

where we have used the condition $\epsilon < M\omega_r^2 r_0^2/2$. In this way, we have obtained the density of states which is the same as Eq. (C2). It is worth noting that two derivations are based on rather different approximations.

1. F. Dalfovo, S. Giorgini, L.P. Pitaevskii, S. Stringari. Theory of Bose–Einstein condensation in trapped gases. *Rev. Mod. Phys.* **71**, 463 (1999).
2. C.J. Pethick, H. Smith. *Bose–Einstein Condensation in Dilute Gases* (Cambridge Univ. Press, 2008) [ISBN: 0 521 66194 3].
3. A. Sinatra, C. Lobo, Y. Castin. Classical-field method for time dependent Bose–Einstein condensed gases. *Phys. Rev. Lett.* **87**, 210404 (2001).

4. M.J. Davis, S.A. Morgan, K. Burnett. Simulations of Bose fields at finite temperature. *Phys. Rev. Lett.* **87**, 160402 (2001).
5. P.B. Blakie, M.J. Davis. Projected Gross–Pitaevskii equation for harmonically confined Bose gases at finite temperature. *Phys. Rev. A* **72**, 063608 (2005).
6. M.J. Davis, S.A. Morgan. Microcanonical temperature for a classical field: Application to Bose–Einstein condensation. *Phys. Rev. A* 68, 053615 (2003).
7. S.J. Rooney, A.J. Allen, U. Zülicke, N.P. Proukakis, A.S. Bradley. Reservoir interactions of a vortex in a trapped three-dimensional Bose–Einstein condensate. *Phys. Rev. A* **93**, 063603 (2016).
8. M.C. Garrett, T.M. Wright, M.J. Davis. Condensation and quasicondensation in an elongated three-dimensional Bose gas. *Phys. Rev. A* **87**, 063611 (2013).
9. S.J. Rooney, T.W. Neely, B.P. Anderson, A.S. Bradley. Persistent-current formation in a high-temperature Bose–Einstein condensate: An experimental test for classical-field theory. *Phys. Rev. A* **88**, 063620 (2013).
10. S.J. Rooney, A.S. Bradley, P.B. Blakie. Decay of a quantum vortex: Test of nonequilibrium theories for warm Bose–Einstein condensates. *Phys. Rev. A* **81**, 023630 (2010).
11. Y.M. Bidasyuk, M. Weyrauch, M. Momme, O.O. Prikhodko. Finite-temperature dynamics of a bosonic Josephson junction. *J. Phys. B: Atomic, Mol. and Opt. Phys.* **51**, 205301 (2018).
12. P.B. Blakie. Numerical method for evolving the projected Gross–Pitaevskii equation. *Phys. Rev. E* **78**, 026704 (2008).
13. A.I. Yakimenko, Y.M. Bidasyuk, M. Weyrauch, Y.I. Kuriatnikov, S.I. Vilchinskii. Vortices in a toroidal Bose–Einstein condensate with a rotating weak link. *Phys. Rev. A* **91**, 033607 (2015).
14. S. Eckel, J.G. Lee, F. Jendrzejewski, N. Murray, C.W. Clark, C.J. Lobb, W.D. Phillips, M. Edwards, G.K. Campbell. Hysteresis in a quantized superfluid 'atomtronic' circuit. *Nature* **506**, 200 (2014).
15. A. Kumar, S. Eckel, F. Jendrzejewski, G.K. Campbell. Temperature-induced decay of persistent currents in a superfluid ultracold gas. *Phys. Rev. A* **95**, 021602 (2017).
16. S.P. Cockburn, N.P. Proukakis. Ab initio methods for finite-temperature two-dimensional Bose gases. *Phys. Rev. A* **86**, 033610 (2012).
17. J. Pietraszewicz, P. Deuar. Classical fields in the one-dimensional Bose gas: Applicability and determination of the optimal cutoff. *Phys. Rev. A* **98**, 023622 (2018).
18. W. Bao, D. Jaksch, P.A. Markowich. Numerical solution of the Gross–Pitaevskii equation for Bose–Einstein condensation. *J. Computat. Phys.* **187**, 318 (2003).
19. M.J. Bijlsma, E. Zaremba, H.T.C. Stoof. Condensate growth in trapped Bose gases. *Phys. Rev. A* **62**, 063609 (2000).
20. K. Snizhko, K. Isaieva, Y. Kuriatnikov, Y. Bidasyuk, S. Vilchinskii, A. Yakimenko. Stochastic phase slips in toroidal Bose–Einstein condensates. *Phys. Rev. A* **94**, 063642 (2016).
21. M. Kunimi, I. Danshita. Decay mechanisms of superflow of Bose–Einstein condensates in ring traps. *Phys. Rev. A* **99**, 043613 (2019).
22. Y. Bidasyuk, W. Vanroose, J. Broeckhove, F. Arickx, V. Vasilevsky. Hybrid method (JM-ECS) combining the J-matrix and exterior complex scaling methods for scattering calculations. *Phys. Rev. C* **82**, 064603 (2010).
23. Y. Bidasyuk, W. Vanroose. Improved convergence of scattering calculations in the oscillator representation. *J. Computat. Phys.* **234**, 60 (2013).

Received 01.02.20

О.О. Приходько, Ю.М. Бідасюк

ПРОЕКТОВАНЕ
РІВНЯННЯ ГРОСА–ПІТАЄВСЬКОГО
ДЛЯ БОЗЕ-ЕЙНШТЕЙНІВСЬКИХ
КОНДЕНСАТІВ КІЛЬЦЕВОЇ ФОРМИ

Запропоновано альтернативну реалізацію проектованого рівняння Гроса–Пітаєвського, адаптовану для атомарних бозе-ейнштейнівських конденсатів у пастках тороїдальної форми. Продемонстровано точну та ефективну схему обчислення матричних елементів і розрахунку часової еволюції хвильової функції конденсату. Проаналізовано точність та стійкість рівноважних і нерівноважних розв'язків для кільцевої пастки з додатковим бар'єром, що відтворює конфігурацію існуючих експериментів.

Ключові слова: бозе-ейнштейнівські конденсати, рівняння Гроса–Пітаєвського, спектральний метод.